J|A|C|S
ARTICLES
Published on Web 07/27/2006

Dynamic Properties of Metallocenium Ion Pairs in Solution by Atomistic Simulations

Andrea Correa and Luigi Cavallo*

Contribution from the Dipartimento di Chimica, Università di Salerno, Via Salvador Allende, Baronissi (SA), I-84081, Italy

Received April 7, 2006; E-mail: lcavallo@unisa.it

Abstract: We report a molecular dynamics study of the dynamics and energetic of the $[H_2Si(Cp)_2ZrMe^+][MeB(C_6F_5)_3^-]$, **IP1**, and $[Me_2Si(Cp)_2ZrMe^+][B(C_6F_5)_4^-]$, **IP2**, ion pairs in benzene. The metrical parameters obtained for the **IP1** ion pair are in excellent agreement with the NMR data reported for the strictly related $[Me_2Si(Cp)_2ZrMe^+][MeB(C_6F_5)_3^-]$ ion pair (*J. Am. Chem. Soc.* **2004**, *126*, 1448). This validates the molecular modeling protocol we developed. Simulation of the **IP2** ion pair suggests that the counterion oscillates between two geometries characterized by a different coordination pattern of the F atoms to the Zr cation. In one case the $B(C_6F_5)_4^-$ coordinates to the metal with two F atoms of the same aryl ring, whereas in the other case two F atoms of different aryl rings are involved in the coordination. Strong solvent reorganization occurs around **IP1** and **IP2**, as well as around the two isolated cations. In the case of the two ion pairs solvent is never coordinated directly to the metal, whereas in the absence of the counterion one benzene molecule is coordinated to the metal through a cation$-\pi$ interaction. Free energy calculations result in ion pair free energies of separation of 36.8 and 23.3 kcal/mol for **IP1** and **IP2**, respectively. Simulations with the Zr−B distance fixed at values > 7 Å have been also performed. This mimics the situation occurring after counterion displacement by an inserting monomer molecule during olefin polymerization by the title catalysts.

Introduction

The evolution of the model of the active species in olefin polymerization catalyzed by group 4 complexes[1−8] (pseudotetrahedral bent metallocenes[9−11] at first, followed by half-metallocenes[12,13] and more recently by nonmetallocene systems such as octahedral phenoxy-amine[14] or phenoxy-imine[15] complexes) can be considered a paradigm for chemistry. Although it was clear enough that the group 4 complex where the chain growth reaction occurs was a cation,[16−18] and that an anionic counterion originated in the activation step should be around, the first models[19−34] simply neglected the anionic counterion (scarcely characterized methyalumoxane at first,[35−41] followed

(1) Brintzinger, H.-H.; Fischer, D.; Mülhaupt, R.; Rieger, B.; Waymouth, R. M. *Angew. Chem., Int. Ed. Engl.* **1995**, *34*, 1143.
(2) Resconi, L.; Cavallo, L.; Fait, A.; Piemontesi, F. *Chem. Rev.* **2000**, *100*, 1253.
(3) Coates, G. W. *Chem. Rev.* **2000**, *100*, 1223.
(4) Makio, H.; Kashiwa, N.; Fujita, T. *Adv. Synth. Catal.* **2002**, *344*, 477.
(5) Mitani, M.; Nakano, T.; Fujita, T. *Chem.—Eur. J.* **2003**, *9*, 2396.
(6) Mitani, M.; Saito, J.; Ishii, S.-I.; Nakayama, Y.; Makio, H.; Matsukawa, N.; Matsui, S.; Mohri, J.; Furuyama, R.; Terao, H.; Bando, H.; Tanaka, H.; Fujita, T. *The Chemical Record* **2004**, *4*, 137.
(7) Coates, G. W.; Hustad, P. D.; Reinartz, S. *Angew. Chem., Int. Ed.* **2002**, *41*, 2236.
(8) McKnight, A. L.; Waymouth, R. M. *Chem. Rev.* **1998**, *98*, 2587.
(9) Ewen, J. A. *J. Am. Chem. Soc.* **1984**, *106*, 6355.
(10) Kaminsky, W.; Külper, K.; Brintzinger, H. H.; Wild, F. R. W. P. *Angew. Chem., Int. Ed. Engl.* **1985**, *24*, 507.
(11) Ewen, J. A.; Jones, R. L.; Razavi, A.; Ferrara, J. D. *J. Am. Chem. Soc.* **1988**, *110*, 6255.
(12) Stevens, J. C.; Timmers, F. J.; Wilson, D. R.; Schmidt, G. F.; Nickias, P. N.; Rosen, R. K.; Knight, G. W.; Lai, S. Y. (Dow Chemical Co.) Eur. Pat. Appl. 416815, 1991.
(13) Stevens, J. C. *Stud. Surf. Sci. Catal.* **1996**, *101*, 11.
(14) Tshuva, E. Y.; Goldberg, I.; Kol, M. *J. Am. Chem. Soc.* **2000**, *122*, 10706.
(15) Fujita, T.; Tohi, Y.; Mitani, M.; Matsui, S.; Saito, J.; Nitabaru, M.; Sugi, K.; Makio, H.; Tsutsui, T. (Mitsui Chemicals) Eur. Pat. Appl. 874005 A1, 1998.
(16) Eisch, J. J.; Piotrowski, A. M.; Brownstein, S. K.; Gabe, E. J.; Lee, F. L. *J. Am. Chem. Soc.* **1985**, *107*, 7219.
(17) Jordan, R. F.; Bajgur, C. S.; Willet, R.; Scott, B. *J. Am. Chem. Soc.* **1986**, *108*, 7410.
(18) Jordan, R. F.; LaPointe, R. E.; Bajgur, C. S.; Echols, S. F.; Willett, R. *J. Am. Chem. Soc.* **1987**, *109*, 4111.
(19) Corradini, P.; Guerra, G.; Vacatello, M.; Villani, V. *Gazz. Chim. Ital.* **1988**, *118*, 173.
(20) Cavallo, L.; Guerra, G.; Vacatello, M.; Corradini, P. *Macromolecules* **1991**, *24*, 1784.
(21) Castonguay, L. A.; Rappé, A. K. *J. Am. Chem. Soc.* **1992**, *114*, 5832.
(22) van der Leek, Y.; Angermund, K.; Reffke, M.; Kleinschmidt, R.; Goretzki, R.; Fink, G. *Chem.—Eur. J.* **1997**, *3*, 585.
(23) Kawamura-Kuribayashi, H.; Koga, N.; Morokuma, K. *J. Am. Chem. Soc.* **1992**, *114*, 8687.
(24) Guerra, G.; Cavallo, L.; Moscardi, G.; Vacatello, M.; Corradini, P. *J. Am. Chem. Soc.* **1994**, *116*, 2988.
(25) Cavallo, L.; Guerra, G. *Macromolecules* **1996**, *29*, 2729.
(26) Guerra, G.; Longo, P.; Cavallo, L.; Corradini, P.; Resconi, L. *J. Am. Chem. Soc.* **1997**, *119*, 4394.
(27) Lohrenz, J. C. W.; Woo, T. K.; Ziegler, T. *J. Am. Chem. Soc.* **1995**, *117*, 12793.
(28) Margl, P.; Lohrenz, J. C. W.; Ziegler, T.; Blöchl, P. E. *J. Am. Chem. Soc.* **1996**, *118*, 4434.
(29) Guerra, G.; Cavallo, L.; Moscardi, G.; Vacatello, M.; Corradini, P. *Macromolecules* **1996**, *29*, 4834.
(30) Yoshida, T.; Koga, N.; Morokuma, K. *Organometallics* **1995**, *14*, 746.
(31) Yoshida, T.; Koga, N.; Morokuma, K. *Organometallics* **1996**, *15*, 766.
(32) Woo, T. K.; Fan, L.; Ziegler, T. *Organometallics* **1994**, *13*, 432.
(33) Fan, L.; Harrison, D.; Woo, T. K.; Ziegler, T. *Organometallics* **1995**, *14*, 2018.
(34) Woo, T. K.; Margl, P. M.; Blöchl, P. E.; Ziegler, T. *J. Am. Chem. Soc.* **1996**, *118*, 13021.
(35) Sinn, H. J.; Kaminsky, W. *Adv. Organomet. Chem.* **1980**, *18*, 99.
(36) Resconi, L.; Bossi, S.; Abis, L. *Macromolecules* **1990**, *23*, 4489.
(37) Sinn, H.; Kaminsky, W.; Hoker, H. *Alumoxanes*; Huthig & Wepf: Heidelberg, Germany, 1995.
(38) Mason, M. R.; Smith, J. M.; Bott, S. G.; Barron, A. R. *J. Am. Chem. Soc.* **1993**, *115*, 4971.
(39) Srinivasa Reddy, S.; Sivaram, S. *Prog. Polym. Sci.* **1995**, *20*, 309.
(40) Siedle, A. R.; Lamanna, W. M.; Newmark, R. A.; Stevens, J.; Richardson, D. E.; Ryan, M. F. *Makromol. Chem., Macromol. Symp.* **1993**, *66*, 215.
(41) Siedle, A. R.; Newmark, R. A. *J. Organomet. Chem.* **1995**, *497*, 119.

10.1021/ja062407v CCC: $33.50 **© 2006 American Chemical Society**

by well-defined organic molecules such as $MeB(C_6F_5)_3^-$ or $B(C_6F_5)_4^-$ derived from boranes and borate salts, respectively[42−49]). Nevertheless, this very simple "cationic model" has been (and still is) used by experimentalists and theoreticians to rationalize and even predict a huge amount of experimental data. The correlation between the symmetry of the group 4 complex and the tacticity of the resulting polymer is an achievement of the cationic model.[19−23,50−52] Regioselectivity of the various catalysts and, in many cases, molecular masses of the resulting polymers have been also rationalized by the cationic model.[23−28,53−55] Nevertheless, in recent years several weaknesses of the cationic model indicated that a step forward had to be made. As an example, the energy barrier for chain growth predicted by the cationic model underestimates by far the experimental value.[27,28] More importantly, a growing body of experimental studies clearly indicated the limits of the cationic model. For instance, the activity of the same group 4 complex is highly dependent on the specific counterion used.[56−70] Similarly, it was shown that the tacticity of polypropylenes produced with C_1- or C_S-symmetric catalysts can be highly tuned by changing the counterion.[61,71] The behavior of the oscillating unbridged metallocenes[72,73] was shown to be strictly related to the specific counterion used.[74, 75]

As common in science, the failure of a simple model (the still extremely useful cationic model) urged the development of new and more sophisticated models that, in this case, explicitly included the anionic counterion. To the best of our knowledge the first modeling of the "ion pair model" appeared in 1997.[76] Although in a simplified way, the counterion was explicitly included to model the chain growth reaction. The ion pair model was subsequently given full credit by several quantum mechanics calculations that investigated in detail different approaches of the monomer to the tightly bound ion pair.[77−85] These studies clearly indicated that the major contribution to the overall energy barrier for chain growth originates from counterion displacement from the cationic center. Of course, excellent experimental activity fundamentally contributed to the development of the ion pair model.[57,86−88] Kinetic studies evidenced that the chain growth reaction cannot be deeply understood without considering a more or less tightly bound ion pair as the propagating species.[56−58,64−70] The microstructure of syndiotactic polypropylenes produced with some C_S-symmetric catalysts could be rationalized only considering competitive isomerization/propagation reactions controlled by the specific counterion.[61]

Thus, it is no surprise that many studies have focused on detailed structural and dynamic characterization of ion pairs in solution.[57,86−92] In particular, NMR techniques were effectively used to investigate several ion pairs containing some typical metallocenes with a family of different counterions. In the case of the $[Me_2Si(Cp)_2ZrMe^+][MeB(C_6F_5)_3^-]$ ion pair it was shown that the tightly bound $MeB(C_6F_5)_3^-$ counterion steadily points the Me group toward the Zr atom.[87] Addition of a Lewis base such as THF to the ion pair solution (to mimic olefin coordination) was also investigated. THF was shown to displace $MeB(C_6F_5)_3^-$ quickly, and the NMR data suggest that after dissociation from the metal $MeB(C_6F_5)_3^-$ no longer points the B−Me bond toward the metal.[87] Far more difficult proved the NMR characterization of the $[Me_2Si(Cp)_2ZrMe^+][B(C_6F_5)_4^-]$ ion pair, due to the weakly coordinating $B(C_6F_5)_4^-$ counterion.[87] Theoretical characterization of ion pairs was also attempted, and quantum mechanics approaches were shown to reproduce well the X-ray structure and rationalized the energetics of ion pair formation of several systems. However, due to the intrinsic static nature of these calculations no dynamical insights could be obtained. The few ab initio molecular dynamics simulations reported are focused on the chain growth reaction.[93,94] Moreover,

(42) Yang, X.; Stern, C.; Marks, T. J. *J. Am. Chem. Soc.* **1991**, *113*, 3623.
(43) Ewen, J. A.; Elder, M. J. (Fina Technology) Eur. Pat. Appl. 427697, 1991.
(44) Chien, J. C. W.; Tsai, W.-M.; Rausch, M. D. *J. Am. Chem. Soc.* **1991**, *113*, 8570.
(45) Ewen, J. A.; Elder, M. J. (Fina Technology) Eur. Pat. Appl. 0426637, 1991.
(46) Turner, H. W. (Exxon Chemical Co.) Eur. Pat. Appl. 0277004 A1, 1988.
(47) Hlatky, G. G.; Upton, D. J.; Turner, H. W. (Exxon Chemical) World Pat. Appl. 91/09882, 1991.
(48) Yang, X.; Stern, C. L.; Marks, T. J. *Organometallics* **1991**, *10*, 840.
(49) Elder, M. J.; Ewen, J. A. (Fina Technology) Eur. Pat. Appl. 0573403, 1993.
(50) Guerra, G.; Cavallo, L.; Corradini, P.; Fusco, R. *Macromolecules* **1997**, *30*, 677.
(51) Milano, G.; Cavallo, L.; Guerra, G. *J. Am. Chem. Soc.* **2002**, *124*, 13368.
(52) Corradini, P.; Guerra, G.; Cavallo, L. *Acc. Chem. Res.* **2004**, *37*, 231.
(53) Toto, M.; Cavallo, L.; Corradini, P.; Moscardi, G.; Resconi, L.; Guerra, G. *Macromolecules* **1998**, *31*, 3431.
(54) Talarico, G.; Busico, V.; Cavallo, L. *J. Am. Chem. Soc.* **2003**, *125*, 7172.
(55) Talarico, G.; Busico, V.; Cavallo, L. *Organometallics* **2004**, *23*, 5989.
(56) Bochmann, M. *J. Organomet. Chem.* **2004**, *689*, 3982.
(57) Song, F.; Lancaster, S. J.; Cannon, R. D.; Schormann, M.; Humphrey, M. B.; Zuccaccia, C.; Macchioni, A.; Bochmann, M. *Organometallics* **2005**, *24*, 1315.
(58) Song, F.; Cannon, R. D.; Lancaster, S. J.; Bochmann, M. *J. Mol. Catal. A: Chem.* **2004**, *218*, 21.
(59) Rodriguez-Delgado, A.; Hannant, M. D.; Lancaster, S. J.; Bochmann, M. *Macromol. Chem. Phys.* **2004**, *205*, 334.
(60) Li, H.; Li, L.; Marks, T. J. *Angew. Chem., Int. Ed.* **2004**, *43*, 4937.
(61) Chen, M.-C.; Roberts, J. A. S.; Marks, T. J. *J. Am. Chem. Soc.* **2004**, *126*, 4605.
(62) Li, H.; Li, L.; Marks, T. J.; Liable-Sands, L. M.; Rheingold, A. L. *J. Am. Chem. Soc.* **2003**, *125*, 10788.
(63) Chen, M.-C.; Marks, T. J. *J. Am. Chem. Soc.* **2001**, *123*, 11803.
(64) Liu, Z.; Somsook, E.; White, C. B.; Rosaaen, K. A.; Landis, C. R. *J. Am. Chem. Soc.* **2001**, *123*, 11193.
(65) Landis, C. R.; Rosaaen, K. A.; Uddin, J. *J. Am. Chem. Soc.* **2002**, *124*, 12062.
(66) Landis, C. R.; Rosaaen, K. A.; Sillars, D. R. *J. Am. Chem. Soc.* **2003**, *125*, 1710.
(67) Sillars, D. R.; Landis, C. R. *J. Am. Chem. Soc.* **2003**, *125*, 9894.
(68) Song, F.; Cannon, R. D.; Bochmann, M. *Chem. Commun.* **2004**, 542.
(69) Song, F.; Cannon, R. D.; Bochmann, M. *J. Am. Chem. Soc.* **2003**, *125*, 7641.
(70) Zhou, J.; Lancaster, S. J.; Walker, D. A.; Beck, S.; Thornton-Pett, M.; Bochmann, M. *J. Am. Chem. Soc.* **2001**, *123*, 223.
(71) Mohammed, M.; Nele, M.; Al-Humydi, A.; Xin, S.; Stapleton, R. A.; Collins, S. *J. Am. Chem. Soc.* **2003**, *125*, 7930.
(72) Coates, G. W.; Waymouth, R. M. *Science* **1995**, *267*, 217.
(73) Lin, S.; Waymouth, R. M. *Acc. Chem. Res.* **2002**, *35*, 765.
(74) Busico, V.; Cipullo, R.; Kretschmer, W. P.; Talarico, G.; Vacatello, M.; Van Axel Castelli, V. *Angew. Chem., Int. Ed.* **2002**, *41*, 505.
(75) Busico, V.; Van Axel Castelli, V.; Aprea, P.; Cipullo, R.; Segre, A. L.; Talarico, G.; Vacatello, M. *J. Am. Chem. Soc.* **2003**, *125*, 5451.
(76) Fusco, R.; Longo, L.; Masi, F.; Garbassi, F. *Macromolecules* **1997**, *30*, 7673.
(77) Lanza, G.; Fragalà, I. L.; Marks, T. J. *Organometallics* **2002**, *21*, 5594.
(78) Lanza, G.; Fragalà, I. L.; Marks, T. J. *Organometallics* **2001**, *20*, 4006.
(79) Lanza, G.; Fragalà, I. L.; Marks, T. J. *J. Am. Chem. Soc.* **1998**, *120*, 8257.
(80) Nifant'ev, I. E.; Ustynyuk, L. Y.; Laikov, D. N. *Organometallics* **2001**, *20*, 5375.
(81) Vanka, K.; Ziegler, T. *Organometallics* **2001**, *20*, 905.
(82) Xu, Z.; Vanka, K.; Firman, T.; Michalak, A.; Zurek, E.; Zhu, C.; Ziegler, T. *Organometallics* **2002**, *21*, 2444.
(83) Xu, Z.; Vanka, K.; Ziegler, T. *Organometallics* **2004**, *23*, 104.
(84) Vanka, K.; Xu, Z.; Ziegler, T. *Can. J. Chem.* **2003**, *81*, 1413.
(85) Vanka, K.; Xu, Z.; Ziegler, T. *Organometallics* **2004**, *23*, 2900.
(86) Stahl, N. G.; Zuccaccia, C.; Jensen, T. R.; Marks, T. J. *J. Am. Chem. Soc.* **2003**, *125*, 5256.
(87) Zuccaccia, C.; Stahl, N. G.; Macchioni, A.; Chen, M.-C.; Roberts, J. A.; Marks, T. J. *J. Am. Chem. Soc.* **2004**, *126*, 1448.
(88) Beringhelli, T.; D'Alfonso, G.; Maggioni, D.; Mercandelli, P.; Sironi, A. *Chem.—Eur. J.* **2005**, *11*, 650.
(89) Beck, S.; Lieber, S.; Schaper, F.; Geyer, A.; Brintzinger, H.-H. *J. Am. Chem. Soc.* **2001**, *123*, 1483.
(90) Schaper, F.; Geyer, A.; Brintzinger, H.-H. *Organometallics* **2002**, *21*, 473.
(91) Lincoln, A. L.; Wilmes, G. M.; Waymouth, R. M. *Organometallics* **2005**, *24*, 5828.
(92) Bryliakov, K. P.; Babushkin, D. E.; Talsi, E. P.; Voskoboynikov, A. Z.; Gritzo, H.; Schroeder, L.; Damrau, H.-R. H.; Wieser, U.; Schaper, F.; Brintzinger, H. H. *Organometallics* **2005**, *24*, 894.
(93) Chan, M. S. W.; Ziegler, T. *Organometallics* **2000**, *19*, 5182.
(94) Yang, S.-Y.; Ziegler, T. *Organometallics* **2006**, *25*, 887.

Chart 1

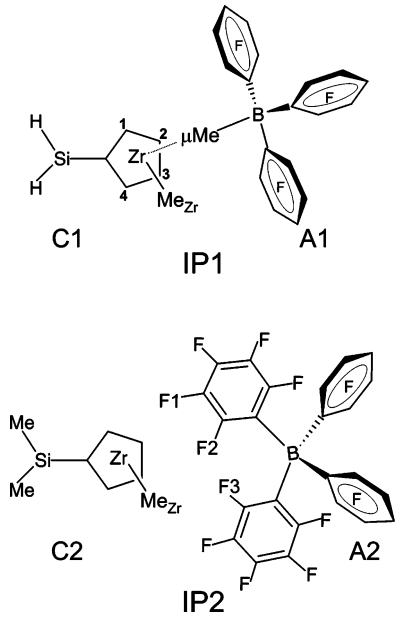

they are in the gas phase and are too short (a few picoseconds) to provide a meaningful sampling of the configuration space.

For this reason, in the context stated by Marks and Macchioni that "*direct structural characterization of the cation−anion interactions in solution (i.e., in the medium in which these catalysts actually function) would greatly facilitate the basic mechanistic understanding of these complex systems*", we decided to develop a modeling protocol to investigate the structure and dynamics of metallocenium ion pairs including explicit solvent. Classic molecular dynamics (MD) based on empirical force fields (largely used for the dynamic and energetic characterization of ion pairs[95−98] and of metals complexes with organics molecules as calixarenes[99,100]) is of course the most appropriate tool, since it allows modelling 10^4-10^5 atoms for simulation times on the order of 10^2-10^3 ns. Indeed, the typical system we model in the following is composed of an ion pair swollen in about 1000 benzene molecules. Quantum mechanics investigations evidenced that the driving force for the cation/anion interaction is mainly electrostatic in nature even in the case of the μMe bridged $MeB(C_6F_5)_3^-$ counterion.[77,101] This allowed us to develop an empirical force field that is able to reproduce with enough accuracy the structure and the energetics of the ion pairs utilized here.[102] The systems we investigated in this manuscript are the $[H_2Si(Cp)_2ZrMe^+][MeB(C_6F_5)_3^-]$, **IP1**, and $[Me_2Si(Cp)_2ZrMe^+][B(C_6F_5)_4^-]$, **IP2**, ion pairs shown in Chart 1.

In the first part of the manuscript we validate our methodology by comparison of our dynamic metrical results for **IP1** with the NMR data of the well characterized and strictly related $[Me_2Si(Cp)_2ZrMe^+][MeB(C_6F_5)_3^-]$ ion pair. After validation, we use the same computational approach to investigate the dynamic behavior of the **IP2** ion pair, whose characterization in solution proved difficult. Then, we report on solvent reorganization around the ion pairs **IP1** and **IP2**, as well as around the isolated cations $H_2Si(Cp)_2ZrMe^+$, **C1**, and $Me_2Si(Cp)_2ZrMe^+$, **C2**, and the isolated anions $MeB(C_6F_5)_3^-$, **A1**, and $B(C_6F_5)_4^-$, **A2**. In the final part we discuss the **IP1** and **IP2** ion pair free energies of separation, as well as the structural changes that occur when the distance between the cation and the anion is increased. This is particularly relevant to understand the possible ion pair reorganization when the counterion is partially displaced by the incoming monomer molecule. The structure of the ion pair after monomer coordination is one of the most intriguing and still unclear sides of the chain growth mechanism. Experimentally, efforts in this direction included the investigation of counterion displacement by competitive coordination of Lewis bases such as phosphines or THF.[87,103] Here we try to contribute toward solving the general problem sharply casted by Busico: "*for a monomer molecule to insert, it is assumed that the anion must be partly displaced, but to where exactly is hard to say*".[75]

Models and Methods

Simulation Details. All simulations were performed in a periodic cubic box using the GROMACS (version 3.2.1) package.[104] Simulations were performed in the isothermal, isobaric (NPT) ensamble. A Berendsen thermostat and a Berendsen barostat were applied to control temperature and pressure.[105] The full system was coupled to a temperature bath at 300 K with a coupling time of 0.2 ps. The pressure was held at 1 atm, with a coupling time of 0.5 ps. Nonbonded interactions were evaluated using a twin-range cutoff. Interactions within the shorter-range cutoff, 15 Å, were evaluated every step, whereas interactions up to the longer cutoff, 20 Å, were updated every five steps together with the nonbonded pair list. To correct for the neglect of the electrostatic interaction beyond the 20 Å cutoff, a reaction field correction with $\epsilon = 2.3$, which is the dielectric constant of benzene at 300 K, was used. Production runs were performed with a time step of 2 fs. Bonds involving hydrogen atoms of solute (ion pairs) and all the bonds of solvent (benzene) were constrained using the SHAKE algorithm.[106] Benzene was described using the force field optimized by Milano and Müller-Plathe.[107]

System Setup and Equilibration. The gas-phase optimized geometries of **IP1**, **IP2**, **C1**, **C2**, **A1**, and **A2** were used as the starting structure for the molecular dynamics simulations. The solute molecule (ion pair or ion) was solvated in a box containing ~1200 molecules of benzene (1091 molecules of benzene for the **IP1**, **C1**, and **A1** systems; 1302 benzene molecules for the **IP2**, **C2**, and **A2** systems). At 1 atm and 300 K these systems correspond to average box lengths of 54 and 59 Å, respectively. The systems were simulated for short intervals at a time step that started from 0.01 fs and was increased to 2 fs. With the final time step, systems were equilibrated for 1.5 ns of MD simulation at constant temperature (300 K) and pressure (1 atm). All simulations were monitored to check for good convergence in terms of energy, temperature, and density, among other properties.

Free Energy Calculation. To investigate the ion pairs at different Zr−B distances we calculated the free energy of the ion pair as a

(95) Wang, L.; Duan, Y.; Shortle, R.; Imperiali, B.; Kollman, P. A. *Prot. Sci.* **1999**, *8*, 1292.
(96) Meng, E. C.; Cieplak, P.; Caldwell, J. W.; Kollman, P. A. *J. Am. Chem. Soc.* **1994**, *116*, 12061.
(97) Yang, Z.-Z.; Li, X. *J. Phys. Chem. A* **2005**, *109*, 3517.
(98) Smith, D. E.; Dang, L. X. *J. Chem. Phys.* **1994**, *100*, 3757.
(99) Miyamoto, S.; Kollman, P. A. *J. Am. Chem. Soc.* **1992**, *114*, 3668.
(100) Blas, J. R.; Marquez, M.; Sessler, J. L.; Luque, F. J.; Orozco, M. *J. Am. Chem. Soc.* **2002**, *124*, 12796.
(101) Lanza, G.; Fragalà, I. L.; Marks, T. J. *J. Am. Chem. Soc.* **2000**, *122*, 12764.
(102) More details can be found in the Supporting Information.
(103) Beck, S.; Prosenc, M. H.; Brintzinger, H.-H. *J. Mol. Catal. A: Chem.* **1998**, *128*, 41.
(104) Van Der Spoel, D.; Lindahl, E.; Hess, B.; Groenhof, G.; Mark, A. E.; Berendsen, H. J. C. *J. Comput. Chem.* **2005**, *26*, 1701.
(105) Berendsen, H. J. C.; Postma, J. P. M.; Van Gunsteren, W. F.; DiNola, A.; Haak, J. R. *J. Chem. Phys.* **1984**, *81*, 3684.
(106) Ryckaert, J. P.; Ciccotti, G.; Berendsen, H. J. C. *J. Comput. Phys.* **1977**, *23*, 327.
(107) Milano, G.; Müller-Plathe, F. *J. Phys. Chem. B* **2004**, *108*, 7415.

function of the ion pair separation, known as the potential of mean force (pmf). The pmf was determined using the coupling parameter approach in conjunction with the thermodynamic integration (TI) formula:[108−110]

$$\Delta G = \int_{\lambda_A}^{\lambda_B} \left\langle \frac{\partial H(\lambda)}{\partial \lambda} \right\rangle_{NPT,\lambda} \partial\lambda \quad (1)$$

In this approach the Hamiltonian H is made a function of a coupling parameter λ. The λ-dependence defines a pathway which connects two states, denoted by A ($\lambda = 0$, initial state) and B ($\lambda = 1$, final state). To solve eq 1, the ensemble average at a number of discrete λ-points was obtained by performing separate simulations for each λ-point, and the integral was determined numerically. In our simulation λ was set as the Zr−B (boron) distance. At each λ-point the Zr−B distance is fixed and the average force along the Zr−B axis is calculated. This average force is subsequently integrated to give the potential of mean force. For both **IP1** and **IP2**, $\lambda = 0$ corresponds to a Zr−B distance of 4.0 Å, while $\lambda = 1$, to a Zr−B distance of 10.0 Å. At each pmf step the Zr−B distance was increases by 0.25 Å, and the systems were first equilibrated for 400 ps and afterward sampled for 1.5 ns.

To approximate the free energy of ion pair separation, ΔG^{Dis}, we used indirect pathways. In this case the coupling parameter approach was used in conjunction with the slow-growth method (SG).[110,111] In the SG method it is assumed that the change in the system from λ_A to λ_B occurs reversibly, such that the system is in equilibrium throughout the entire change. The coupling parameter is then made a function of time, and the ensemble average of eq 1 is replaced by a derivative evaluation of ΔG^{Dis} at each point of MD simulation, according to the formula of eq 2, which follows from the assumption of reversibility.

$$\Delta G^{Dis} = \sum_{i=1}^{N_{MD}} \left(\frac{\partial H(\lambda)}{\partial \lambda} \right)_i \Delta\lambda \quad (2)$$

In our case the initial state λ_A corresponds to the tightly bound ion pairs, while the final state λ_B corresponds to the isolated cations and counterions. The final state can be reached by combining slow annihilation of the cation (or counterion) from the tightly bound ion pair and from a solvent box with the isolated cation (or counterion). In this case the λ parameter corresponds to the nonbonded parameters of solute (van der Waals parameters and point charges). λ was changed with a rate of 5×10^{-7} for the time step (2 fs), for a total simulation time of 4 ns for each transformation. Further details can be found in the Results and Discussion section.[102]

Results and Discussion

Structural Characterization. The system containing **IP1** as solute (see Chart 1) was equilibrated for 1.5 ns and then sampled for 3 ns. The behavior of the Zr−B and Zr−μMe distances was monitored over the sampling time, and the corresponding distribution functions, DFs, are displayed in Figure 1a and in Figure 1b, respectively. Both DFs show one peak only at 4.2 ± 0.1 and 2.5 ± 0.1 Å for Zr−B and Zr−μMe, respectively, corresponding to the contact ion pair. These two values are in very good agreement with the values of the Zr−B and Zr−μMe distances, 4.20 and 2.55 Å, respectively, observed in the X-ray structure of the strictly related $[Cp_2ZrMe^+][MeB(C_6F_5)_3^-]$ system.[112] The DFs of the distances between the μMe group and the four hydrogen atoms of the Cp ligands, also reported in Figure 1, present one peak only as well. The order of μMe−H distances, μMe−H4 ≫ μMe−H3 > μMe−H1 > μMe−H2, reproduces well the trend determined by NMR experiments both qualitatively and quantitatively. Noteworthy, the μMe−H4 DF is centered at quite a larger distance with respect to those calculated for the H1, H2, and H3 atoms, in agreement with the absence of detectable NMR signals between the μMe group and the H4 proton.[87] Similar good agreement between the calculated and the experimental values is obtained for several other metrical parameters; see Table 1. As regards the relative orientation of the $H_2Si(Cp)_2ZrMe^+$ cation and the $MeB(C_6F_5)_3^-$ counterion, the average Zr−μMe−B angle from the MD simulation, 175° ± 4°, indicates that the $MeB(C_6F_5)_3^-$ counterion steadily points the Me−B bond toward the Zr atom, as found in the X-ray structure of the metallocenium contact ion pair containing the $MeB(C_6F_5)_3^-$ counterion,[112,113]

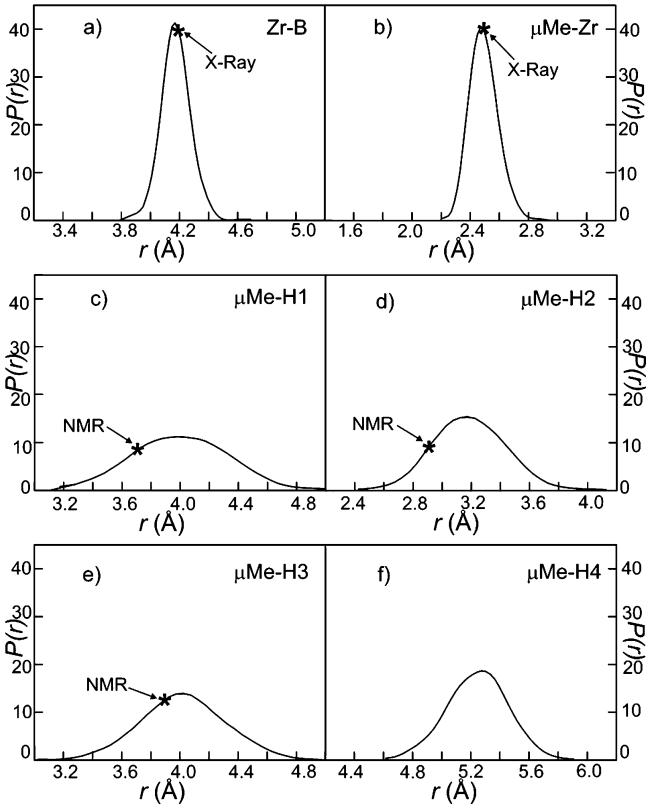

Figure 1. Distribution function, DF, of several geometric parameters in the **IP1** system.

Table 1. Comparison between Calculated and Experimental Geometrical Parameters of **IP1**; Distances in Å, Angles in deg

parameter	MD	NMR or X-ray
μMe−H1	4.00 ± 0.32	3.7[a]
μMe−H2	3.42 ± 0.25	3.0[a]
μMe−H3	4.10 ± 0.28	3.9[a]
μMe−H4	5.30 ± 0.20	
Zr−B	4.20 ± 0.09	4.20[b]
Zr−μMe	2.50 ± 0.09	2.55[b]
o-F−H1	4.36 ± 1.21	4.7[a]
o-F−H2	3.77 ± 1.21	4.1[a]
o-F−H3	5.21 ± 0.97	5.1[a]
Me_{Zr}−H3	3.44 ± 0.24	3.1[a]
Me_{Zr}−H4	3.14 ± 0.11	3.2[a]
Zr-Me-B	175 ± 4	169[b]

[a] NMR value from ref 87. [b] X-ray value from ref 112.

(108) Kirkwood, J. G. *J. Chem. Phys.* **1935**, *3*, 300.
(109) van Gunsteren, W. F.; Beutler, T. C.; Fraternali, F.; King, P. M.; Mark, A. E.; Smith, P. E. *Comput. Simul. Biomol. Syst., Vol. 2* **1993**, 315.
(110) King, P. M. *Comput. Simul. Biomol. Syst., Vol. 2* **1993**, 267.
(111) Chipot, C.; Kollman, P. A.; Pearlman, D. A. *J. Comput. Chem.* **1996**, *17*, 1112.
(112) Guzei, I. A.; Dagorne, S.; Jordan, R. F. *Acta Crystallogr., Sect. C* **2001**, *C57*, 143.

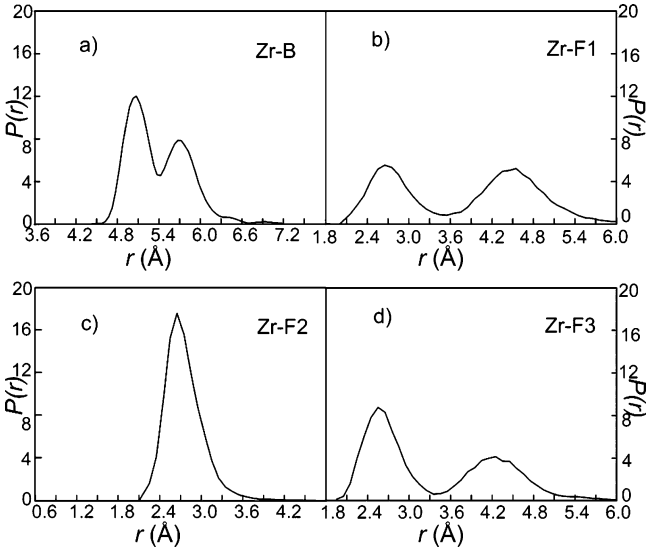

Figure 2. Distribution function, DF, of several geometric parameters in the **IP2** system.

and is in agreement with the dynamical NMR structure of $[Me_2Si(Cp)_2ZrMe^+][MeB(C_6F_5)_3^-]$.[87]

These results are of relevance for two reasons. First, they support the NMR analysis. In fact, many geometrical parameters obtained from analysis of the NMR spectra of $[Me_2Si(Cp)_2ZrMe^+][MeB(C_6F_5)_3^-]$ were derived on the assumption that the average *o*-F−μMe and Me_{Zr}−H3 distances in solution are substantially equal to the same distances in the X-ray structure of the $[(Cp)_2ZrMe^+][MeB(C_6F_5)_3^-]$ ion pair.[112] Second, the consistency among the X-ray structure, the NMR analysis, and the MD simulations strongly validates the MD approach as a useful tool for the structural and dynamic characterization of metallocenium ion pairs in solution. This can be particularly useful where NMR experiments are of difficult rationalization, as in the case of weakly coordinating counterions such as the $B(C_6F_5)_4^-$ system we discuss next.

Since the **IP2** ion pair (see Chart 1) is characterized by a weaker cation−anion interaction with respect to **IP1**, we extended the sampling time from 3 to 6 ns. This allowed a more accurate sampling of the flexible dynamic behavior of **IP2**. The DF of the Zr−B distance (see Figure 2a) shows a bimodal behavior with a first peak around 5.0 Å and a second peak around 5.7 Å. Analysis of the Zr−F distances indicates that bimodal behavior is also presented by the DF of the Zr−F1 and Zr−F3 distances (see Figure 2b and Figure 2d) that present a first peak around 2.7 Å and a second peak around 4.5 Å. Alternatively, the DF of the Zr−F2 distance presents unimodal behavior.

A plot of the Zr−F1 and Zr−F3 distances vs time shows almost perfect complementarity; see Figure 3. Thus, the bimodal behavior of the DF of the Zr−B distance corresponds to oscillation of **IP2** between two different geometries. The first maximum, around Zr−B ∼5 Å, can be associated with a structure in which coordination to the Zr atom occurs through two *o*-F atoms of different aryl rings (structure *o*-F,*o*-F, Figure 3b). The second maximum, around Zr−B ∼5.7 Å, can be associated with a structure in which coordination to the Zr atom occurs through an *o*-F and a *m*-F atom of the same aryl ring (structure *o*-F,*m*-F, Figure 3c). The cation−anion interaction of the *o*-F,*m*-F structure is quite similar to the X-ray structure of the $[(Me_5Cp)_2ThMe^+][B(C_6F_5)_4^-]$ ion pair (Th−*o*-F = 2.76 Å, Th−*m*-F = 2.67 Å).[114] The average persistence time of **IP2** in each geometry is about 600 ps. Analysis of the Zr−F2 distance vs time indicates that rearrangement between the *o*-F,*o*-F and the *o*-F,*m*-F structures does not require dissociation of F2 from the metal.

Solvent Structuration. To understand solvent reorganization around the ion pairs as well as around the isolated ions, we performed four additional MD simulations corresponding to the isolated cations $H_2Si(Cp)_2ZrMe^+$, **C1**, and $Me_2Si(Cp)_2ZrMe^+$, **C2**, and isolated anions $MeB(C_6F_5)_3^-$, **A1**, and $B(C_6F_5)_4^-$, **A2**.

The radial distribution function of the benzene center of mass, CM_{Sol}, with respect to the B atom from the MD simulation of **IP1** and **A1**, $g^{B}_{IP1}(r)$ and $g^{B}_{A1}(r)$, respectively, are shown in Figure 4a, while the corresponding CM_{Sol} radial distribution functions from the MD simulation of **IP2** and **A2**, $g^{B}_{IP2}(r)$ and $g^{B}_{A2}(r)$, respectively, are shown in Figure 4b. Visual inspection of Figure 4 clearly indicates that rather similar solvent structuration occurs around the ion pairs **IP1** and **IP2** and the isolated counterions **A1** and **A2**. Solvent structuration is slightly reduced in the ion pairs relative to the isolated counterions, as expected on going from a neutral ion pair to a charged counterion. Rather different, instead, is the behavior of the radial distribution function of CM_{Sol} with respect to the Zr atom from the MD simulation of **IP1** and **C1**, $g^{Zr}_{IP1}(r)$ and $g^{Zr}_{C1}(r)$, respectively, as well as from the MD simulation of **IP2** and **C2**, $g^{Zr}_{IP2}(r)$ and $g^{Zr}_{C2}(r)$, respectively; see Figure 4c and Figure 4d. The peak around 3.0 Å in $g^{Zr}_{C1}(r)$ and $g^{Zr}_{C2}(r)$ clearly indicates that remarkable solvent structuration occurs around the isolated cations. This peak is completely absent in $g^{Zr}_{IP1}(r)$ and $g^{Zr}_{IP2}(r)$. Integration of both $g^{Zr}_{C1}(r)$ and $g^{Zr}_{C2}(r)$ until the first minimum is the average number of Zr-coordinated benzene molecules. In both cases 1.1 benzene molecules coordinate to the metal in the absence of the counterion. Of course, classical cation-π interaction is the driving force for this interaction.[115−118] Analysis of the residence time[119,120] indicates that a benzene molecule remains coordinated to the metal for about 70 ps, on the average, before being displaced by another benzene molecule. Insight into the average coordination geometry of the benzene to the Zr cation can be obtained from the DF of the Me_{Zr}−Zr−CM_{Sol} and Si−Zr−CM_{Sol} angles obtained from the benzene molecules with the CM_{Sol} within 3.5 Å from the metal in **C1**; see Figure 5. While the Me_{Zr}−Zr−CM_{Sol} angle is well centered at 90 ± 10°, the Si−Zr−CM_{Sol} angle is spread in the range 120°−160°, which indicates a rather large mobility of the benzene and of the Me_{Zr} group in the equatorial belt of the uncrowded $H_2Si(Cp)_2Zr$ metallocene. The average structure of **C1** with a coordinated benzene molecule is that reported in Figure 5c.

The peak at $r \geq 10$ Å in the radial distribution functions of Figure 4 indicates that solvent structuration involves at least two solvation spheres and occurs up to quite large distances from the metal, which is consistent with the low polarity of the

(113) Yang, X.; Stern, C.; Marks, T. J. *J. Am. Chem. Soc.* **1994**, *116*, 10015.
(114) Jia, L.; Yang, X.; Stern, C. L.; Marks, T. J. *Organometallics* **1997**, *16*, 842.
(115) Ma, J. C.; Dougherty, D. A. *Chem. Rev.* **1997**, *97*, 1303.
(116) Dougherty, D. A. *Science* **1996**, *271*, 163.
(117) Gapeev, A.; Dunbar, R. C. *J. Am. Chem. Soc.* **2001**, *123*, 8360.
(118) Gokel, G. W.; De Wall, S. L.; Meadows, E. S. *Eur. J. Org. Chem.* **2000**, 2967.
(119) Lounnas, V.; Pettitt, B. M. *Proteins: Struct., Funct., Genet.* **1994**, *18*, 148.
(120) De Simone, A.; Dodson, G. G.; Verma, C. S.; Zagari, A.; Fraternali, F. *Proc. Natl. Acad. Sci. U.S.A.* **2005**, *102*, 7535.

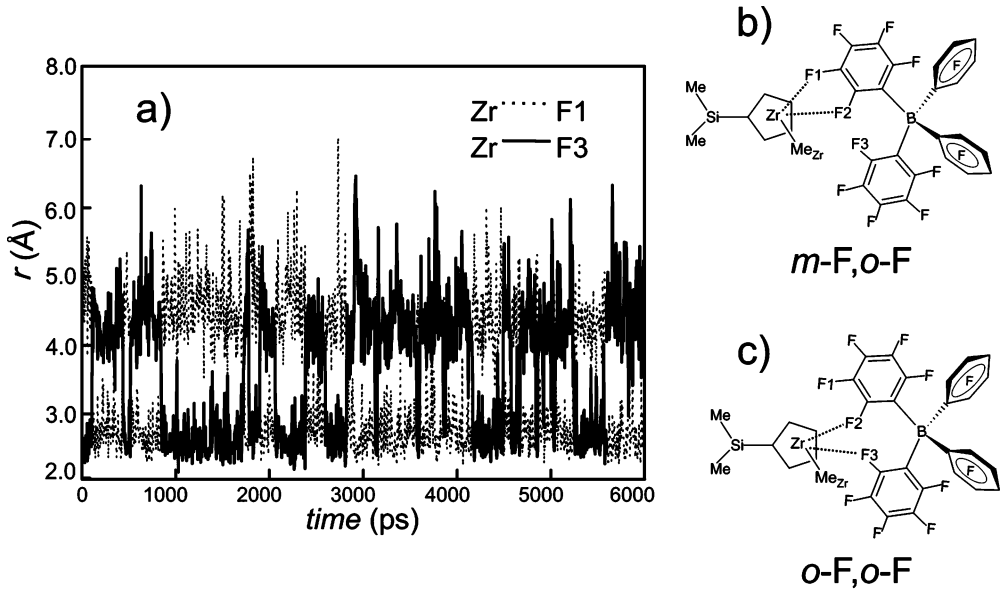

Figure 3. Plot vs time of the Zr−F1 and Zr−F3 distances. The two low-energy structures from MD simulation of **IP2** are also shown.

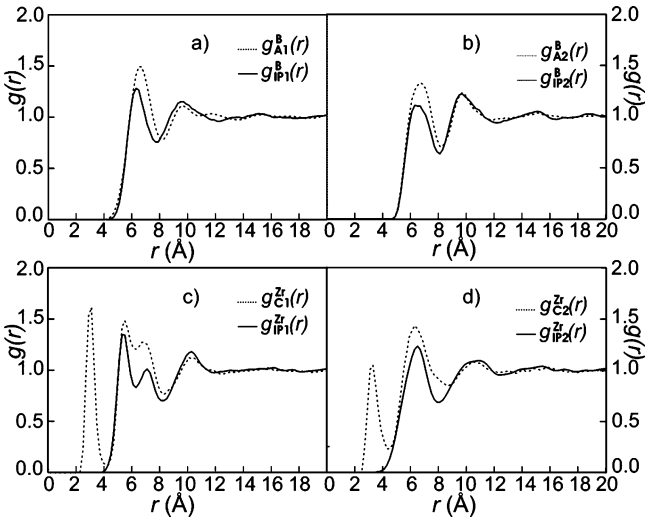

Figure 4. Radial distribution functions of the benzene center of mass with respect to the following: (a) the B atom of **IP1** and **A1**; (b) the B atom of **IP2** and **A2**; (c) the Zr atom of **IP1** and **C1**; (d) the Zr atom of **IP2** and **C2**.

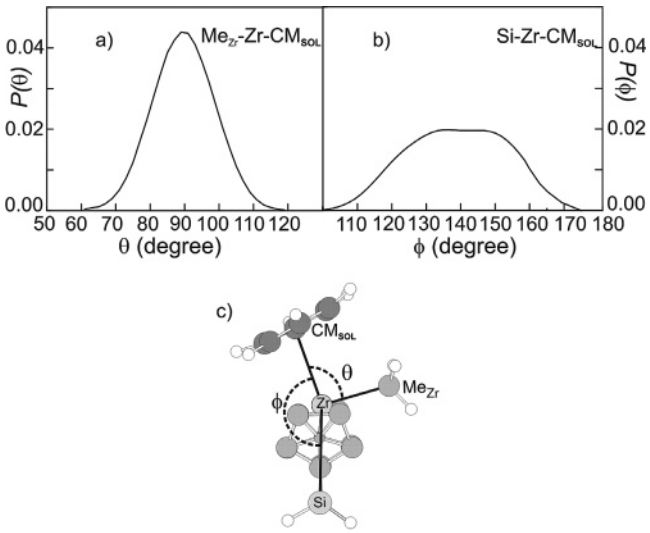

Figure 5. DF of the Me_{Zr}−Zr−CM_{Sol} (a) and Si−Zr−CM_{Sol} (b) angles. Average structure for a benzene molecule coordinated to **C1** (c).

solvent. Integration of $g^{Zr}_{C1}(r)$ until $r \approx 8$ Å and until $r \approx 11$ Å indicates that 15.0 and 24.3 benzene molecules, respectively, participate to the first and second coordination sphere of **C1**. Similar results were obtained for **C2**. Finally, it is noteworthy that in the MD simulations of **IP1** and **IP2** no sign of substitution/displacement of the counterion by a solvent molecule was observed. While this is expected for the tightly bound **IP1** ion pair, it was less predictable in the case of the weakly bound **IP2** ion pair.

Dynamics and Energetic of Ion Pair Dissociation. The free energy of dissociation (or separation) of **IP1**, ΔG^{Dis}_{IP1}, can be approximated following either of the two thermodynamic paths shown in Scheme 1. Both paths are two-step paths. The former path is associated with metallocene annihilation. The basis of this approach rests in the fact that the free energy G is a thermodynamic state function. This mean that as long as a system in equilibrium is changed in a reversible way the change in free energy, ΔG, will be independent of the path. The power of this approach lies in the fact that on a computer also nonchemical processes, such as the annihilation of a molecule or group of molecules, may be performed in order to obtain ΔG of a certain process.[109]

Specifically, in our case step 1 corresponds to annihilation of the metallocene from **IP1** (i.e., **IP1** → **A1** mutation), and it is followed by step 2 which corresponds to annihilation of **C1** in a solvent box (i.e., **C1** → **Solvent-box** mutation). The difference in the free energy values calculated for the two steps is one approximation to ΔG^{Dis}_{IP1}. The latter path, instead, is associated with counterion annihilation (i.e., **IP1** → **C1** mutation followed by **A1** → **Solvent-box** mutation), and a different estimate of ΔG^{Dis}_{IP1} is obtained. A similar procedure can be applied to evaluate the free energy of dissociation of **IP2**, ΔG^{Dis}_{IP2}. The values of ΔG^{Dis}_{IP1} and ΔG^{Dis}_{IP2} obtained following the paths of Scheme 1 are reported in Table 2.

It is clear that for both **IP1** and **IP2** the free energies of ion pair separation obtained following either of the two alternative

(121) Vanka, K.; Chan, M. S. W.; Pye, C. C.; Ziegler, T. *Organometallics* **2000**, *19*, 1841.

Scheme 1

Cation annihilation

$$\text{Step 1: } [A^- C^+]_{Sol} \rightarrow [A^-]_{Sol} + \Delta G^{C}_{1}$$

$$\text{Step 2: } [C^+]_{Sol} \rightarrow [\ ]_{Sol} + \Delta G^{C}_{2}$$

Step 1 - Step 2

$$[A^- C^+]_{Sol} + [\ ]_{Sol} \rightarrow [A^-]_{Sol} + [C^+]_{Sol}$$

$$\Delta G^{Dis}_{IP1} = \Delta G^{C}_{1} - \Delta G^{C}_{2}$$

Anion annihilation

$$\text{Step 1: } [A^- C^+]_{Sol} \rightarrow [C^+]_{Sol} + \Delta G^{A}_{1}$$

$$\text{Step 2: } [A^-]_{Sol} \rightarrow [\ ]_{Sol} + \Delta G^{A}_{2}$$

Step 1 - Step 2

$$[A^- C^+]_{Sol} + [\ ]_{Sol} \rightarrow [A^-]_{Sol} + [C^+]_{Sol}$$

$$\Delta G^{Dis}_{IP1} = \Delta G^{A}_{1} - \Delta G^{A}_{2}$$

Table 2. Free Energies of Ion pair Separation and Hysteresis, in kcal/mol, for the Processes Shown in Scheme 1

system	process	ΔG^{Dis}_{IPn}	hysteresis
IP1	metallocene annihilation	35.1	1.2
	counterion annihilation	38.5	1.8
IP2	metallocene annihilation	22.6	2.1
	counterion annihilation	23.9	1.1

paths are very similar, which supports the validity of the procedure. Moreover, the paths of Scheme 1 can be also traced backward (i.e., creating the metallocene or the counterion). The free energy difference between the values obtained from forward and backward tracing of the paths of Scheme 1 is known as hysteresis, and it is an estimate of the error associated with the transformation considered. The low hysteresis values reported in Table 2 again support the procedure we followed. Moreover, the average ΔG^{Dis}_{IP1} and ΔG^{Dis}_{IP2} we obtained, 36.8 and 23.3 kcal/mol, respectively, are in good agreement with the enthalpy of ion pair separation in toluene, 38.0 and 22.1 kcal/mol, calculated by Ziegler and co-workers for the (1,2-[$(Me_2Cp)_2ZrMe^+$][$MeB(C_6F_5)_3^-$] and [$(1,2\text{-}Me_2Cp)_2ZrMe^+$][$B(C_6F_5)_4^-$] ion pairs, respectively, using a DFT approach.[121] Although MD free energies and DFT enthalpies are compared, the good agreement between the ion pair separation energies obtained with totally different computational approaches is a remarkable cross-validation of both approaches and, on the other hand, suggests that the entropic contribution is small. Of course, in the framework that the main energy barrier to chain growth is counterion displacement from the tightly bound ion pair,[56,78−80,83] the high ΔG^{Dis}_{IP1} we calculated is in agreement with the low activity experimentally shown by metallocene systems when activated by borane cocatalysts such as $B(C_6F_5)_3$.[57] Consistently, the quite lower ΔG^{Dis}_{IP2} we calculated is in agreement with the higher activity experimentally shown by the same metallocene when borate salts such as [Ph_3C^+][$B(C_6F_5)_4^-$] are used as activators.[57]

To investigate the dynamics and energetics of **IP1** and **IP2** at larger cation−anion distances, we performed a potential of mean force (pmf) calculation along the Zr−B distance; see Models and Methods. The corresponding curves are sketched in Figure 6. The pmf of **IP1** exhibits a very steep behavior with only one minimum around 4 Å that corresponds to the tightly bound ion pair. Instead, the pmf of **IP2** shows smoother behavior. The two minima around 5.0 and 5.7 Å correspond to the *o*-F,*o*-F, and *o*-F,*m*-F structures of Figure 3, respectively. These two minima are separated by a free energy barrier of about 1 kcal/mol only. Furthermore, the pmf of **IP2** shows a very shallow minimum around 7.5−8.0 Å that corresponds to the outer sphere ion pair. This conclusion is supported by analysis of the $g^{Zr}_{IP2}(r)$ at increasing Zr−B distances, reported in Figure 7. For the sake of consistency a similar analysis was performed for the **IP1** ion pair.

Up to Zr−B distances equal to 6 Å, the overall shape of both $g^{Zr}_{IP1}(r)$ and $g^{Zr}_{IP2}(r)$ is very similar to that for the tightly bound ion pairs **IP1** and **IP2** of Figure 4. At a Zr−B distance equal to 6.25 Å a small shoulder appears in both $g^{Zr}_{IP1}(r)$ and $g^{Zr}_{IP2}(r)$. This shoulder evolves into a peak when increasing the Zr−B distance to 7.0 Å. At Zr−B = 7.25 Å the overall shape of both $g^{Zr}_{IP1}(r)$ and $g^{Zr}_{IP2}(r)$ is very similar to that of $g^{Zr}_{C1}(r)$ and $g^{Zr}_{C2}(r)$ reported for the naked cations **C1** and **C2** in Figure 4, with the newly formed peak around 3 Å. Integration of the new peak corresponds to a coordination number of 1.1 benzene molecules. This clearly indicates that at Zr−B > 7 Å a benzene molecule replaces the anion in the first coordination sphere of Zr. Formation of the outer sphere ion pair at Zr−B distances just longer than 7 Å is in excellent agreement with the average Zr−B distance of 7.2−7.3 Å determined by NMR experiments for the [$Me_2Si(Cp)_2ZrMe^+$][$MeB(C_6F_5)_3^-$] ion pair after addition of THF.[87] Interestingly, only a rather short elongation of the Zr−B distance (from 4.2 to 6.75 Å for **IP1**, and from 5−5.5 to 6.75 Å for **IP2**) is needed to allow a solvent molecule to be inserted between the cation and the anion to form an outer sphere ion

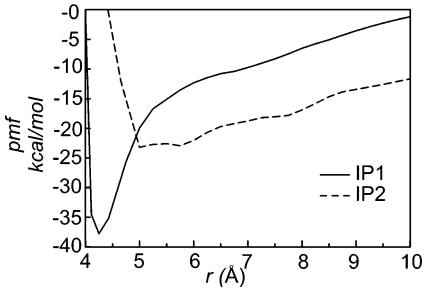

Figure 6. **IP1** and **IP2** potential of mean force in benzene as a function of the Zr−B distance. The minima of the curves have been shifted to the average ΔG^{Dis} values from the slow growth simulations.

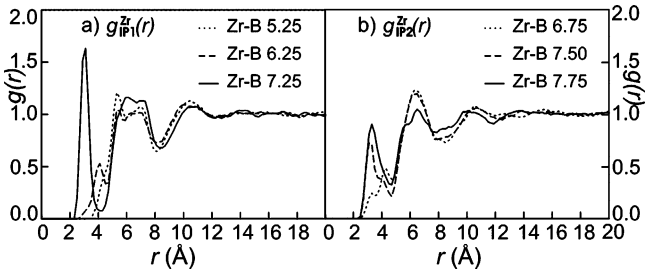

Figure 7. Radial distribution function (at various Zr−B distances) of the solvent around the Zr atom of **IP1** and **IP2**.

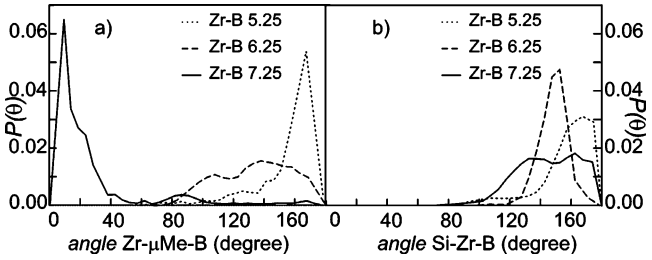

Figure 8. Distribution function of the Zr−μMe−B (a) and Si−Zr−B (b) angles at various Zr−B distances, for the **IP1** ion pair.

pair. The pmf's of Figure 6 indicate that this small counterion displacement is less favored for **IP1** compared to **IP2**.

Finally, structural analysis of **IP1** and **IP2** at large Zr−B distances, when the outer sphere ion pair is formed, can also contribute to rationalization of the position assumed by the counterion during the chain growth step (i.e., after displacement by the inserting monomer molecule). This is one of the still unsolved questions of this kind of catalysis. DF of the Zr−μMe−B angle of **IP1** at various Zr−B distances, reported in Figure 8, indicates that at increasing Zr−B distances the counterion rotates considerably. At Zr−B distances > 7 Å, i.e., in the outer sphere ion pair, the counterion is completely rearranged. The B−Me bond points away from the metal (Zr−μMe−B $\approx$ 0°), while the three C_6F_5 groups face the metallocene. Thus, our results support the "hat-like" orientation of the cation−anion pair that Zuccaccia et al. suggested to be adopted by the $[Me_2Si(Cp)_2ZrMe^+][MeB(C_6F_5)_3^-]$ ion pair after addition of THF.[87]

Conclusions

In this manuscript we reported on the structure, dynamics, and energetics of the $[H_2Si(Cp)_2ZrMe^+][MeB(C_6F_5)_3^-]$ and $[Me_2Si(Cp)_2ZrMe^+][MeB(C_6F_5)_4^-]$ ion pairs. In the case of the former ion pair we obtained excellent agreement with NMR dynamic and X-ray static structural data of the very strictly related $[H_2Si(Cp)_2ZrMe^+][MeB(C_6F_5)_3^-]$ and $[(1,2\text{-}Me_2Cp)_2ZrMe^+][MeB(C_6F_5)_3^-]$ ion pairs. We further investigated the free energy of ion pair dissociation, and in quantitative agreement with previous quantum mechanics calculations, we found that the borane-based counterion binds much more strongly than the borate-based counterion to the cationic metallocene. This is in qualitative agreement with the higher activity experimentally exhibited by metallocenes when activated by borate salts, compared to the same systems activated by borane.

These results strongly validate the simulation protocol and support the predictive power of the methodology. Indeed, in the case of the $[Me_2Si(Cp)_2ZrMe^+][B(C_6F_5)_4^-]$ ion pair, where experimental data are difficult to rationalize, our simulations indicate that the tightly bound ion pair oscillates between (at least) two geometries with a different Zr...F interaction pattern. In one case coordination occurs with two F atoms of the same perfluorinated aryl ring, while in the other case coordination involves two F atoms of different perfluorinated aryl rings. Moreover, we could investigate in detail the severe solvent reorganization that occurs around the tightly bound ion pairs as well as around the naked cation and anions. The analysis also indicated that in the case of the isolated cations one benzene molecule coordinates strongly to the metal through a typical cation−π interaction. The coordinated benzene molecule shows a residence time of about 70 ps on the average, before being displaced by another solvent molecule.

Finally, we shed light on the energetics and dynamics of outer sphere ion pair formation. Our analysis clearly indicates that a rather short elongation of the Zr−B distance is needed (about 2−3 Å) in order for a solvent molecule to snake between the cation and the anion to form an outer sphere ion pair. In the case of the $MeB(C_6F_5)_3^-$ counterion, formation of the outer sphere ion pair results in a severe rearrangement of the cation/counterion geometry. In fact, the B−Me bond no more points toward the Zr atom. We believe it is not hazardous to speculate that a similar behavior could be exhibited in the chain growth step, when a monomer molecule has to displace the counterion.

Finally, we believe that the very good agreement between our simulations and the available experimental data indicates that the approach we developed can be safely extended to investigate the dynamics and energetics of ion pairs with nonmetallocene-based catalysts and, more in general, of any metallorganic ion pair. Moreover, it can be also used as a complementary tool in the NMR characterization of metallorganic ion pairs. In this respect, we recall that tightly bound ion pairs are relevant intermediates in a large number of reactions catalyzed by organometallic complexes. However, the first extension of this approach will be the investigation of metallocenium ion pairs when the Me group bound to the Zr atom is replaced by a much longer alkyl group (to simulate more reliably the growing chain) and when the simple *ansa*-Cp_2 ligands considered here are replaced by more complex systems such as isospecific C_2-symmetric and syndiospecific C_S-symmetric metallocenes.

Acknowledgment. We thank Dr. G. Milano, University of Salerno, and Dr. D. Roccatano, International University Bremen, for useful suggestions and discussions. This work was supported by the MURST of Italy (PRIN 2004), CINECA (Progetti di Supercalcolo convenzione CINECA/INSTM), University of Salerno (Grant Medie Apparecchiature 2002) and by Basell Polyolefins.

Supporting Information Available: Details on the force field parametrization and on the free energy calculations. Energies and optimized geometries for all the DFT-calculated structures, used in the force field development. This material is available free of charge via the Internet at http://pubs.acs.org.

JA062407V